Journal of American Science

Websites:
http://www.jofamericanscience.org
http://www.sciencepub.net

Emails:
editor@sciencepub.net
sciencepub@gmail.com

MARSLAND PRESS
Multidisciplinary Academic Journal Publisher

Effect of insulin and captopril on diabetic cardiomyopathy in adult male albino rat: Histological, biochemical and pharmacological study

Radwa Mohammed Ahmed[1], Asmaa Mohammed Mohammed Ibrahim[2], Mohamed Hussein Elmahdi[3], Mostafa Yehia Abdelwahed[4], Ayman Mohamed Helal[5], Mohamed Mahmoud Sofi[1]

[1] Anatomy and Embryology Department, Faculty of Medicine, Fayoum University, Egypt
[2]Biochemistry and Molecular Biology Department, Faculty of Medicine, Fayoum University, Egypt
[3] Pathology Department, Faculty of Medicine, Fayoum University, Egypt
[4] Physiology Department, Faculty of Medicine, Fayoum University, Egypt
[5] Pharmacology Department, Faculty of Medicine, Fayoum University, Egypt

Abstract: Introduction: Diabetic cardiomyopathy is characterized by structural and functional myocardial alterations. hyperglycaemia is a major contributing factor in its pathogenesis. So, insulin therapy is mandatory in diabetic patients. Angiotensin converting enzyme inhibitors (ACEIs) e.g. captopril, may play a beneficial role in management of diabetic cardiomyopathy. However, combined insulin and captopril therapy is much more effective in attenuation of severe cardiac damage exerted by oxygen free radicals released in diabetic patients via different mechanism most probably due to hyperglycaemia. **Aim of work**: to elucidate the protective role of insulin and captopril on diabetes mellitus induced histological alterations in myocardium of adult male albino rat. **Material and methods**: This research used 50 adult male albino rats weighing 180-220 g. The rats were classified into five groups 10 rats each: Group I (Normal control): The rats of this group were injected intravenously once with 0.9% saline. Group II (Diabetic Control): The rats of this group were injected once with STZ intravenously into the tail vein on a 40 mg / kg dose. Group III (Insulin-treated Diabetic rats): The rats of this group were injected subcutaneously with insulin once daily at 2 U / kg body weight dose after induction of diabetes mellitus for six weeks. Group IV (Diabetic rats treated with captopril): The rats of this group were administered with captopril by oral gavage at a 100mg / kg body weight dose once daily for six weeks after diabetes mellitus induction Group V (Diabetic rats treated with insulin and captopril): The rats of this group rats received a combined treatment of insulin at a dose of 2U/ kg/day and captopril 100 mg/kg by the same previously mentioned routes. **Results:** Examination of specimens of diabetic rats revealed markedly disturbed myocardial architecture, mononuclear cell infiltration, cytoplasmic degeneration and extensive fibrosis. Insulin and captopril co-administration markedly ameliorated these histological alterations more than using insulin or captopril alone.

[Radwa Mohammed Ahmed, Asmaa Mohammed Mohammed Ibrahim, Mohamed Hussein Elmahdi, Mostafa Yehia Abdelwahed, Ayman Mohamed Helal, Mohamed Mahmoud Sofi. **Effect of insulin and captopril on diabetic cardiomyopathy in adult male albino rat: Histological, biochemical and pharmacological study.** *J Am Sci* 2020;16(8):93-109]. ISSN 1545-1003 (print); ISSN 2375-7264 (online). http://www.jofamericanscience.org. 10. doi:10.7537/marsjas160820.10.

Key words: Diabetic cardiomyopathy, insulin, captopril, heart.

1. Introduction:

Diabetes mellitus a major health problem associated with cardiovascular diseases and cardiac mortality. Diabetic cardiomyopathy is characterized by structural and functional myocardial alterations; myocardial apoptosis and fibrosis mainly due to oxidative stress and DNA damage. The myocardium is very sensitive to damaging effect of reactive oxygen species (ROS) because of its highly oxidative metabolism and deficient antioxidant defence mechanisms **(Westermann et al, 2009; Falcoa-Pires et al, 2012 and Zheng et al, 2019).**

Singh et al, 2008 reported that insulin therapy is mandatory in diabetic patients especially those who developed diabetic cardiomyopathy in order to reduce blood glucose level. They added that hyperglycaemia is a major contributing factor in the pathogenesis of diabetic cardiomyopathy and release of ROS in myocardial tissue.

Angiotensin converting enzyme inhibitors (ACEIs) are widely used for cardiovascular disease treatment; congestive heart failure, hypertension and myocardial infarction. In diabetic cardiomyopathy, hyperglycemia causes overproduction of the mitochondrial superoxide, which contributes to ROS

activation. The role of the renin-angiotensin system in the pathogenesis of diabetic cardiomyopathy has been proved in different animal studies. Diabetes mellitus is distinguished by high angiotensin converting enzyme (ACE) activity, that transforms angiotensin I (ANG-I) to angiotensin II (ANG-II), a powerful oxidative agent, and inactivates bradykinin involved in antioxidant defensive system. So, ACE inhibition can be proposed as playing a critical role in preventing oxidative stress and DNA damage. **(Munzel and Keaney, 2001; Abuissa et al, 2005; Andraws and Brown, 2007; McGuire et al, 2008; Mikrut et al, 2016).**

A significant mediator of neovascularization in physiological and pathophysiological conditions is the vascular endothelial growth factor (VEGF); with important roles in the formation of developmental blood vessels and regulation of tissue angionenesis caused by hypoxia. Uncontrolled VEGF-induced angiogenesis in the retinal microvascular tissue may cause pathological neovascularisation. VEGF expression in diabetic patients is reported to be upregulated in retina and renal glomeruli. However, decreased expression of VEGF and its receptors in cardiac tissue in those patients resulted in insufficient collateral vascular development in ischemia response and increased cardiovascular morbidity and death rates in patients with diabetes (**Chou et al, 2002).**

2. Material and methods:

Chemicals:

1- Streptozotocin (STZ): (Sigma, St. Louis, Missouri, USA): rats were injected with STZ intravenously once into the tail vein at a dose of 40mg/kg.

2- Insulin: Was obtained from (Egyptian Drug Trading Company, The Egyptian Pharmaceutical Trading Company, 1353, Corniche El-Nil, Shobra, Cairo, Egypt). It was available as glass vials namely Insulin mixtard. It was injected subcutaneously at a dose of 2 U/kg once daily.

3- Captopril: was obtained from (L.L.C; SmithKline Beecham, Cairo, Egypt). It was available as 25mg tablets (Capoten 25 mg tablets).

Induction of diabetes mellitus: Was done by injection of a single dose of 40 mg/kg body weight of Streptozotocin (STZ). after 12 h of diabetes mellitus was confirmed by measuring the fasting blood glucose level (Accu-Chek Active blood glucose meter; Roche Diagnostic, Mannheim, Germany) on days 3 and 5 after induction of diabetes mellitus. Rats with fasting blood glucose level greater than 250 mg/dl for two consecutive measurements were confirmed as diabetic **(Wen et al, 2008 and Balkis et al, 2009).**

Animals and experimental design:

Fifty adult male albino rats weighing 180-220 g were used in this study. They were obtained from the animal house, Faculty of Medicine, Cairo University. The rats were housed in separate cages and maintained under standard laboratory and environmental conditions with standard rat chow. The rats were divided into five groups 10 rats each:

Group I (**Normal control**): The rats of this group were injected intravenously once with 0.9% saline.

Group II (Diabetic Control): The rats of this group were injected once with STZ intravenously into the tail vein at a dose of 40 mg/ kg **(Wen et al, 2008 and Balkis et al, 2009).**

Group III (Diabetic rats treated with insulin): The rats of this group were injected subcutaneously with insulin once daily at a dose of **2 U**/ kg body weight after induction of diabetes mellitus for six weeks (**Shiju et al, 2012).**

Group IV (Diabetic rats treated with captopril): The rats of this group were administered with captopril by oral gavage at a dose of **100**mg/ kg body weight after induction of diabetes mellitus once daily for six weeks (**Michael et al, 2012).**

Group V (Diabetic rats treated with insulin and captopril): The rats of this group rats received a combined treatment of insulin at a dose of 2U/ kg/day (**Benter et al, 2011)** and captopril 100 mg/kg by the same previously mentioned routes.

Cervical dislocation was done to all rats six weeks after confirmation of diabetes mellitus. Rats were treated in accordance with the ethical guidelines approved by the animal committee of Cairo University.

Methods:

The heart was excised and processed for the following studies:

1- Light microscopic study using hematoxylin and eosin and Masson´ trichrome stains. (**Calvi et al, 2012)**:

A- Haematoxylin and eosin stain:

The muscle tissues were fixed in 4% para-formaldehyde. The histological sections were deparaffinized in xylene, rehydrated through a graded series of ethanol, and washed in running water. The sections were then immersed in Harris' hematoxylin for two minutes, washed in running water (five minutes), rinsed in distilled water (one minute), stained in an aqueous solution of eosin (five minutes), and dehydrated in ascending concentrations of ethanol. Next, the sections were cleared in xylene (three successive changes, one minute each) and mounted under a cover-slip.

B- Masson's trichrome staining*:*

The histological sections were deparaffinized, rehydrated, washed in running water (two minutes),

immersed in 5% iron alum (ten minutes) and Regard's hematoxylin (three minutes), and rinsed in distilled water, 95% alcohol, and picric alcohol. Then, the sections were washed again in running water (ten minutes), rapidly immersed in xylidine ponceau aqueous solution (three minutes), distilled water and 1% glacial acetic acid, and 1% phosphomolybdic acid (three minutes). Next, they were rinsed again in distilled water, immersed in aniline blue for 2-5 minutes, dehydrated, cleared, and mounted under a cover-slip.

2- Electron microscopic examination: **Transmission electron microscopy (TEM) study (Esteva et al, 2008):**

Small cylinders (4 mm long x×1 mm x1 mm) of tissue were prepared from each equatorial heart section. These heart tissue samples were fixed by immersion in vials which contained 1 mL of mixed solution glutaraldehyde 1.25% and paraformaldehyde 1% in a phosphate-buffered saline (PBS) buffer solution, at 4°C for 48 h. Samples were washed with PBS 0.14M (pH = 7.4) for 45 min. This process was repeated three times. Subsequent steps were carried out by the Serveis Cientifico-Tècnics (SCT) of the Universitat de Barcelona. In the SCT, samples were subjected to a post-fixation process in osmium tetraoxide (OsO4) 1% in PBS for 1 h. Samples were then dehydrated in acetone. They were left in different solutions with ascending acetone concentrations for 10 min. Dehydrated samples were mounted in Spurr's epoxide resin blocks. The resin blocks were cut and semithin sections (1.5µm) were processed. These sections were then observed with an optic microscope at 40× to choose the regions of interest for processing and analysing using TEM. The chosen regions were cut and put into square and eyelet grids. They were contrasted so that they could be studied with TEM.

3- Antioxidant enzymes: Cardiac glutathione peroxidise (GSP) and super oxide dismutase (**SOD): (Neamati et al, 2013)**

Measurement of SOD activity

The activity of superoxide dismutase (SOD) was evaluated with Randox SOD detection kit according to the manufacturer's instructions. The role of SOD is to accelerate the dismutation of the toxic superoxide (O^{2-}) produced during oxidative energy processes to hydrogen peroxide and molecular oxygen. This method employs xanthine and xanthine oxidase to generate superoxide radicals which react with 2-(4-iodophenyl)-3-(4-nitrophenol)-5-phenyltetrazolium chloride (I.N.T.) to form a red formazan dye. The SOD activity is then measured by degree of inhibition of this reaction. One unit of SOD is that which causes 50% inhibition of the rate of reduction of INT under the conditions of the assay. SOD levels were recorded at 505 nm and through a standard curve and expressed as unit per milligram of tissue protein (unit/mg protein).

Measurement of GSH **activity**

The activity of glutathione peroxidase (GSH) was evaluated with Randox GSH detection kit according to the manufacturer's instructions. GSH catalyse the oxidation of glutathione by cumene hydroperoxide. In the presence of glutathione reductase (GR) and NADPH, the oxidised glutathione (GSSG) is immediately converted to the reduced form with a concomitant oxidation of NADPH to NADP+. The decrease in absorbance was measured spectrophotometrically (S2000 UV model; WPA, Cambridge, UK) against blank at 340 nm. One unit (U) of GSH was defined as 1 µmol of oxidized NADPH per min per milligram of tissue protein. The GSH activity was expressed as unit per milligram of tissue protein (unit/mg protein).

Real time polymerase chain reaction (PCR) analysis of vascular endothelial growth factor **(VEGF)** - mRNA in rat myocardium, kidney and retina: **Real-time Quantitative RT-PCR (RT-qPCR)**: **(Liu et al, 2011; Patel and Thaker 2015):** Total RNA was purified using the RNeasy mini kit (Qiagen, Valencia, CA), and cDNA was synthesized using the iScriptc DNA synthesis kit (Bio-Rad) with 0.5 _g of total RNA according to the manufacturer's recommendations. qPCR was performed with primers specific for VEGF, and GAPDH using iQ SYBR Green Supermix in an iQ5 real-time PCR detection system (Bio-Rad). The primers were designed and ordered from Integrated DNA Technologies (Coralville, IA), and primer sequences used were as follows: VEGF, 5_-GTTCACTGTGAGCCTTGTTCAG-3_ (forward) and 5_-GTCACATCTGCAAGTACGTTCG-3_ (reverse); and GAPDH, 5_-CTGGAGAAACCTGCCAAGTA-3_ (forward) and 5_-TGTTGCTGTAGCCGTATTCA-3_ (reverse). Pilot real-time RT-qPCR experiments were performed to determine optimal condition for each primer. All real-time RT- qPCR experiments were performed in duplicate. The primer specificity of the amplification product was confirmed by melting curve analysis of the reaction products using SYBR Green as well as by visualization on ethidium bromide-stained agarose (1.5%) gels. The housekeeping gene GAPDH was used as an internal control, and gene-specific mRNA expression was normalized against GAPDH expression. iQTM5 optical system software (Bio-Rad; version 2.0) was used to analyze real-time RT-qPCR data and derive threshold cycle (CT) values according to the manufacturer's instructions.

3. Results:

Histological results:

Group I (Normal control):

Light microscopic inspection of rat heart specimens stained with haematoxylin and eosin stain showed normal myocardial architecture; branching and anastomizing of cardiac muscle fibres with oval vesicular nuclei running in various directions and acidophilic sarcoplasm, spindle shaped nuclei of fibroblast in the interstitial tissue in-between and small thin walled blood vessels **(Figs. 1,2,3).** Sections of the normal control rat heart, stained with Masson's trichrome visualized a normal pattern of collagen deposition-a thin layer of collagen tissue between myocardial fibers and around blood vessels **(Fig. 4).** Electron microscopic examination of rat heart specimens of the same group revealed euchromatic nucleus with prominent nucleoli, numerous branching cardiac muscle fibers with numerous mitochondria between myofibrils, alternating dark bands and light bands with regular Z lines inside and sarcomere between 2 successive z lines **(Figs. 5, 6).**

Group II (Diabetic Control):

Light microscopic examination of rat heart specimens stained with haematoxylin and eosin stain showed mononuclear cell infiltration, markedly thickened and congested blood vessels, markedly disturbed myocardial architecture with disrupted myocardial fibers, widening of interstitial spaces, markedly increased fibroblasts, pyknotic and karyolitic nuclei. Sarcoplasm vaculation of myocardial fibers can be visualized **(Figs. 7,8,9).** Sections of the of the same group stained with Masson's trichrome visualized a marked increase in collagen tissue deposition between myocardial fibers and around blood vessels **and** an extensively fibrosed segment of rat myocardium (**Figs. 10,11).**

Electron microscopic examination of rat heart specimens of the same group revealed markedly disturbed or completely lost myocardial architecture with disrupted myofibrils, extensive sarcoplasmic rarefaction and extremely shrunken karyolitic nuclei. Ballooned mitochondria with lost cristae could be observed **(Figs. 12,13,14).**

Group III (Diabetic rats treated with insulin):

Light microscopic examination of rat heart specimens stained with haematoxylin and eosin stain showed apparently normal pattern of myocardial fibers, fairly widened interstitial spaces, moderately thickened blood vessel, mildly increased fibroblasts and extravasted blood, Few areas of sarcoplasmic vacuolation with few karyolitic and Pyknotic nuclei could be seen **(Figs. 15,16).** Sections of the same group stained with Masson's trichrome visualized moderate increase in collagen tissue deposition between myocardial fibers and around a markedly congested blood vessel **(Fig. 17).**

Electron microscopic examination of rat heart specimens of the same group revealed some apparently normal myofibrils; a sarcomer between two successive Z lines, disrupted myofibrils, extensive sarcoplasmic rarefaction. Pathological aggregation of mitochondria that are apparently normal with intact cristae or ballooned with lost cristae.

Group IV (Diabetic rats treated with captopril):

Light microscopic examination of rat heart specimens stained with haematoxylin and eosin stain showed markedly widened interstitial spaces and increased fibroblasts, a moderately congested blood vessel, disrupted myocardial fibers, mononuclear cell infiltration, around a thickened blood vessel. Sarcoplasmic vacuolation, pyknotic and karyolitic nuclei could be visualized **(Figs. 19,20).**

Sections of the same group, stained with Masson's trichrome visualized marked increase in collagen tissue deposition between myocardial fibers and around blood vessels **(Fig.21).**

Electron microscopic examination of rat heart specimens of the same group revealed extremely shrunken and karyolitic nucleus, marked sarcoplasmic rarefaction, some apparently normal myoibrils;, apparently normal myoibrils; alternating dark bands and light bands with regular Z lines inside and a sarcomere between 2 successive Z lines. The mitochondria are either apparently normal with intact cristae or mostly ballooned with lost cristae **(Figs. 22,23).**

Group V (Diabetic rats treated with insulin and captopril):

Light microscopic examination of rat heart specimens stained with haematoxylin and eosin stain showed apparently normal pattern of myocardial fibers and their nuclei, Few spindle shaped nuclei of fibroblasts in the interstitial tissue in-between and small thin walled blood vessels. Few areas of sarcoplasmic vacuolation could be seen **(Fig.24).** Sections of the same group, stained with Masson's trichrome visualized apparently normal distribution of in collagen tissue between myocardial fibers and around blood vessels **(Fig.25).**

Electron microscopic examination of rat heart specimens of the same group revealed euchromatic nucleus with a prominent nucleolus (n)apparently normal myocardial architecture; alternating dark bands and light bands with regular Z lines inside and sarcomere between 2 successive Z lines. Most of mitochondria were apparently normal with intact cristae and few of them were ballooned with lost cristae **(Figs. 26, 27, 28).**

Statistical analysis of data:

Using SPSS software statistical computer package version 22 (SPSS Inc, USA), the data collected were arranged, tabulated and analysed statistically. Calculation was made of the mean and standard deviation. ANOVA (Variance Analysis) was

used to evaluate the difference between groups regarding mean values of calculated parameters, multiple comparisons were made using Tukey HSD among pairs of groups (Post hoc range test). Significance was adopted at $P \leq 0.05$ for interpretation of test results of significance. As regards **collagen area present**, there was a statistically significantly difference in group II, III and IV when compared to control, $p < 0.0001$, 0.001 and <0.0001, respectively. However, no statistically significant difference ($p = 0.870$) between group V and group I. Additionally, in group III, IV and V, there was a statistically significant difference relative to group II, respectively, p<0.0001, 0.016 and < 0.0001. Also, the difference between group III and V was statistically significant, p=0.006. But between Group III and Group IV ($p = 0.150$) there was no statistically significant difference. On the other hand, the difference between group IV and group V was statistically significant ($p < 0.0001$) **(Figs. 29, 30).**

Concerning **glutathione peroxidise (GPD),** there was a statistically significantly difference in group II, III, IV and V when relative to control, $p < 0.0001$, <0.0001,<0.0001and 0.024, respectively. As well as, there was a statistically significantly difference in group III, IV and V as relative to group II, $p < 0.0001$. Also, there was a statistically significantly difference in group IV and group V relative to group III, p=0.011 and 0.008, respectively. The difference between group IV and group V was statistically significant ($p < 0.0001$) **(Figs.31, 32).**

Regarding **Superoxide dismutase (SOD),** there was a statistically significantly difference in group II, III, IV and V when relative to control, $p < 0.0001$, <0.0001, <0.0001and 0.002, respectively. As well as, there was a statistically significantly difference in group III, IV and V as relative to group II, $p < 0.0001$. Furthermore, the difference between group V and group III was statistically significant, p=0.001. But, no statistically significant difference was found between group III and group IV (p=0.067). The difference between group IV and group V was statistically significant ($p < 0.0001$) **(Figs.33, 34).**

Heart VEGF was statistically significantly higher in group III (2.44 ± 0.51), and V (5.39 ± 0.54) compared to control (1.28± 0.35), p =0.006 and p<0.0001, respectively. However, no statistically significant difference was found between group II and IV with control, p=0.116 and 0.183, respectively. Also, it was statistically significantly higher in group III (2.44 ± 0.51), IV (1.96 ± 0.55) and V (5.39 ± 0.54) compared to group II (0.53 ± 0.31), p<0.0001, p=0.001, and $p < 0.0001$, respectively. Also, Heart VEGF was statistically significantly higher in group V (5.39 ± 0.54) compared to group III (2.44 ± 0.51), $p < 0.0001$. But, no statistically significant difference was found between group III and group IV ($p = 0.481$). Also, a statistically significant difference was found between group IV and group V ($p < 0.0001$) **(Figs. 35, 36)**

Kidney VEGF was statistically significantly higher in group II (4.01 ± 0.29), III (2.40 ± 0.38), IV (3.16± 0.51), and V (1.87± 0.15) when compared to control (0.94± 0.23), p<0.0001, <0.0001, <0.0001 and p =0.003, respectively. On the other hand, it was a statistically significantly lower in group III (2.40 ± 0.38), IV (3.16 ± 0.51), and V (1.87 ± 0.15) compared to group II (4.01 ± 0.29), p<0.0001, p=0.005, and $p < 0.0001$, respectively. Kidney VEGF was statistically significantly higher in group IV (3.16 ± 0.51) compared to group III (2.40 ± 0.38), p =0.014. But, no statistically significant difference was found between group III and group V ($p = 0.134$). However, a statistically significant difference was found between group IV and group V ($p < 0.0001$) **(Figs. 37, 38)**

Retina VEGF was statistically significantly higher in group II (3.94± 0.13), III (2.66± 0.43), and IV (3.02± 0.6) when compared to control (0.96± 0.21), p<0.0001. However, there was no a statistically significant difference between group V with control, p=0.098. On the other hand, it was a statistically significantly lower in group III (2.66± 0.43), IV (3.02± 0.6), and V (1.62± 0.38) compared to group II (3.94± 0.13), p<0.0001, p=0.013, and $p < 0.0001$, respectively. Retina VEGF was statistically significantly higher in group V (1.62± 0.38) compared to group III (2.66± 0.43), p =0.004. But, there was no statistically significant difference between the group III and group IV ($p = 0.603$). However, there was a statistically significant difference between the group IV and group V ($p < 0.0001$) **(Figs. 39, 40)**

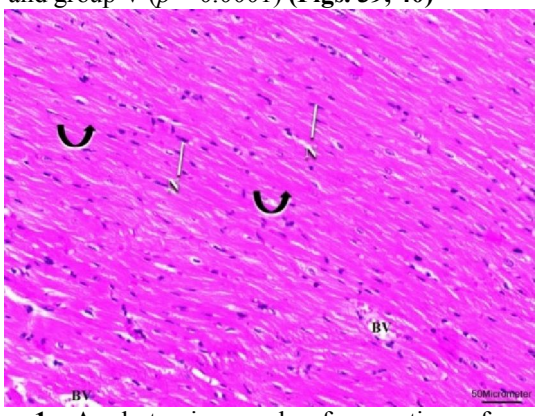

Fig. 1: A photomicrograph of a section of a rat myocardium from group I (Normal control) showing normal architecture of myocardium; branching and anastomosing cardiac muscle fibers (curved arrow) running in different directions with oval vesicular nuclei (N) and acidophilic sarcoplasm. Small thin walled blood vessels can be observed **(H & E X200).**

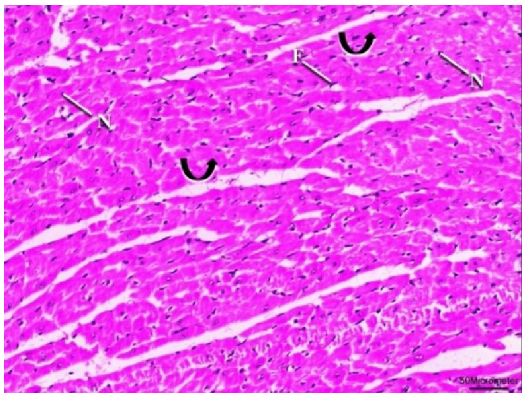

Fig. 2: A photomicrograph of a transverse section of a rat myocardium from group I showing normal architecture of myocardium; branching and anastomosing cardiac muscle fibers (curved arrow) running in different directions with oval vesicular nuclei (N) and acidophilic sarcoplasm. Few spindle shaped nuclei of fibroblast in the interstitial tissue in-between (F) can be observed **(H & E X200).**

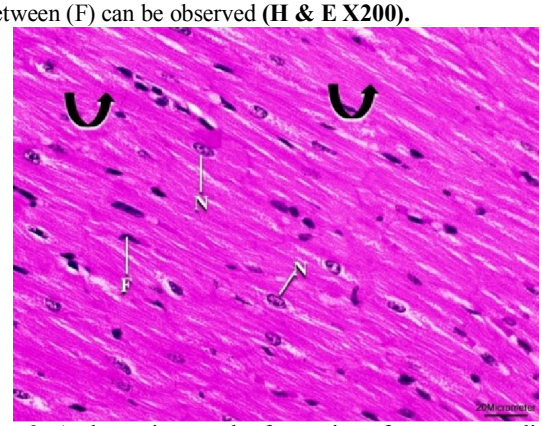

Fig. 3: A photomicrograph of a section of a rat myocardium from group I showing normal architecture of myocardium; branching and anastomosing cardiac muscle fibers (curved arrow) running in different directions with oval vesicular nuclei (N) and acidophilic sarcoplasm. Few spindle shaped nuclei of fibroblast in the interstitial tissue in-between (F) can be observed **(H & E X400).**

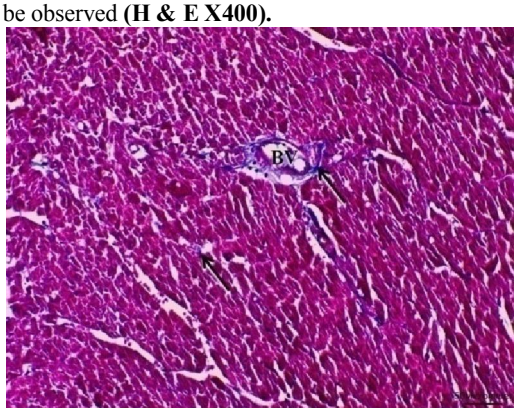

Fig. 4: A photomicrograph of a section of a rat myocardium from group I displaying normal architecture of myocardium with minimal collagen deposition (arrow) between myocardial fibers and around blood vessels **(BV) (Masson's trichrome x 200).**

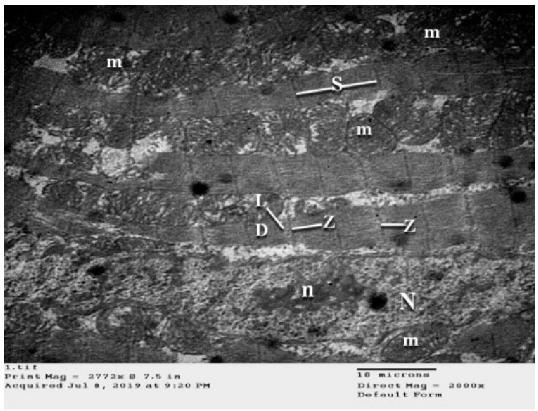

Fig. 5: An electron micrograph of a section of rat myocardium from group I showing euchromatic nucleus (N) with prominent nucleoli (n), numerous mitochondria (m) between myofibrils alternating dark bands (D) and light bands (L) with regular Z lines inside and sarcomere (S) between 2 successive z lines **(TEM x20000).**

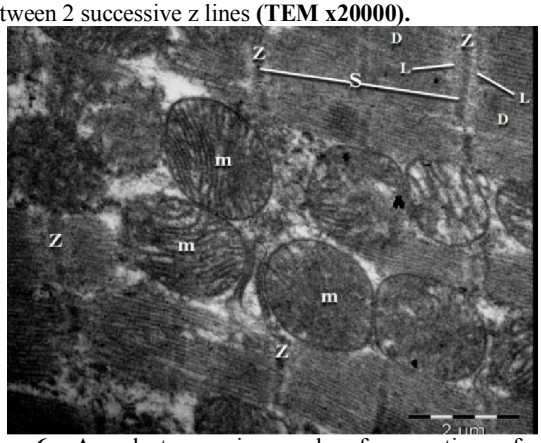

Fig. 6: An electron micrograph of a section of rat myocardium from group I showing alternating dark bands (D) and light bands (L) with regular Z lines inside and sarcomere (S) between 2 successive z lines **(TEM x18000).**

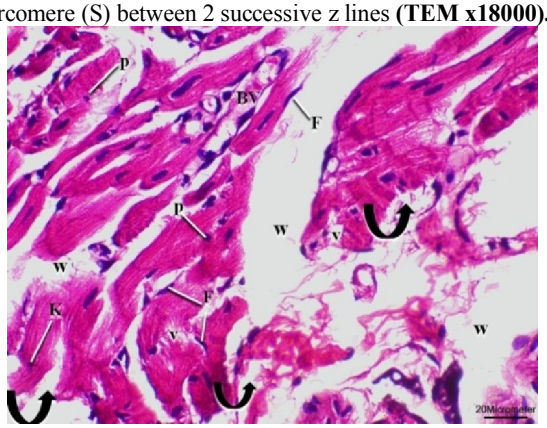

Fig. 7: A photomicrograph of a section of a rat myocardium from group II **(Diabetic Control):** showing markedly disturbed myocardial architecture with disrupted myocardial fibers (curved arrow), widening of interstitial spaces (W), markedly increased fibroblast (F), pyknotic (p) and karyolitic nuclei (K). Sarcoplasm vaculation (v) of myocardial fibers can be visualized. **(Hx. & E.X400).**

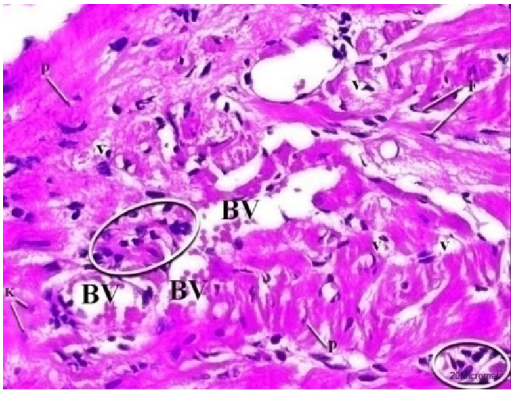

Fig. 8: A photomicrograph of a section of a rat myocardium from group II**:** showing markedly disturbed myocardial architecture with mononuclear cell infiltration (Inf), markedly thickened and congested blood vessels (BV) pyknotic (p) and karyolitic (K) nuclei. Markedly increased fibroblast in the interstitial spaces (F) and sarcoplasm vaculation (v) of myocardial fibers can be visualized. **(Hx. & E.X400).**

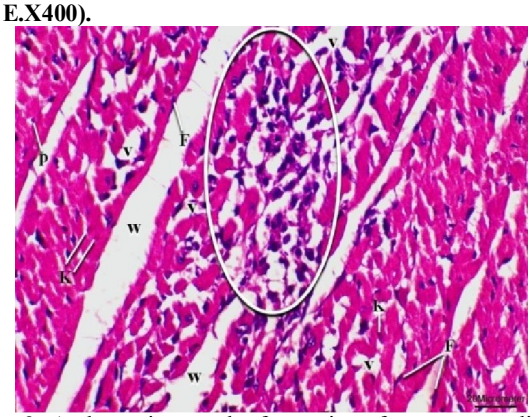

Fig. 9: A photomicrograph of a section of a rat myocardium from group II**:** showing markedly widened interstitial spaces (W), disturbed myocardial architecture with sever mononuclear cell infiltration (Inf), pyknotic (p) and karyolitic (K). nuclei Markedly increased fibroblast in the interstitial spaces (F) and sarcoplasm vaculation (v) of myocardial fibers can be visualized. **(Hx. & E.X400).**

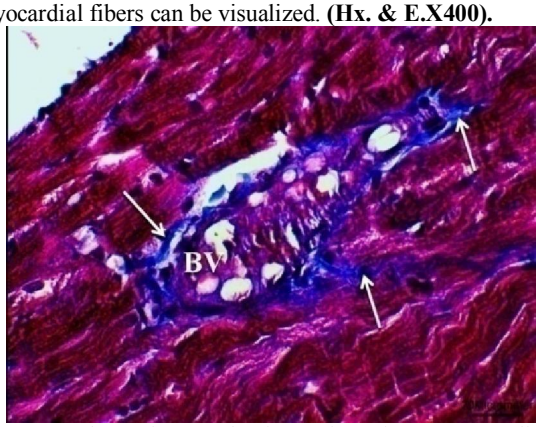

Fig.10: A photomicrograph of a section of a rat myocardium from group II displaying marked increase in collagen tissue deposition (arrow) between myocardial fibers and around blood vessels **(BV) (Masson's trichrome x 400)**

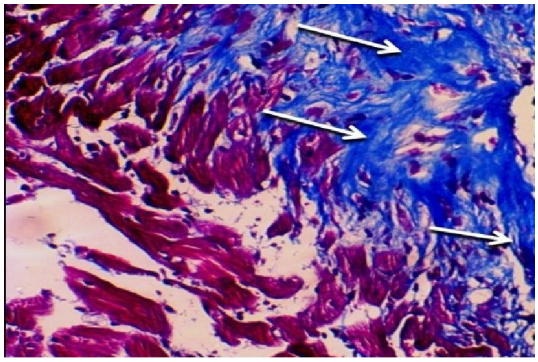

Fig.11: A photomicrograph of a section from group II displaying an extensively fibrosed segment of rat myocardium (arrow) **(Masson's trichrome x 200).**

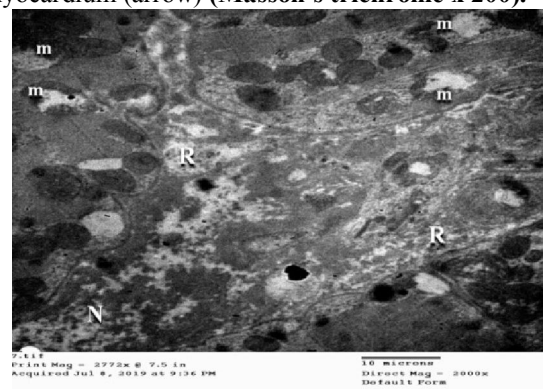

Fig.12: An electron micrograph of a section of a rat myocardium from group II showing markedly disturbed myocardial architecture with extensive sarcoplasmic rarefaction (R) and karyolitic nucleus (N). Most of mitochondria appear ballooned with lost cristae (m) **(TEM X2000)**

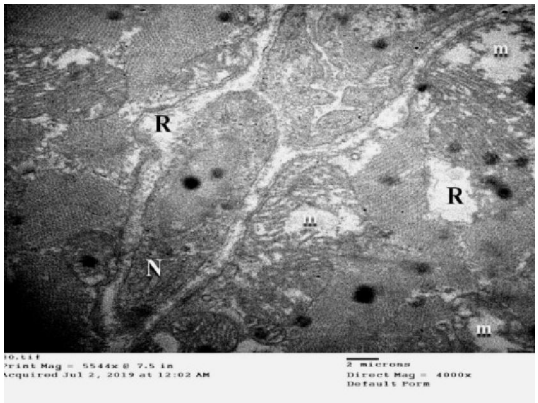

Fig.13: An electron micrograph of a section of a rat myocardium from group II showing completely lost normal pattern of myocardial architecture with extensive sarcoplasmic rarefaction (R) and extremely shrunken and karyolitic nucleus (N). Most of mitochondria appear ballooned with lost cristae (m) **(TEM X4000)**

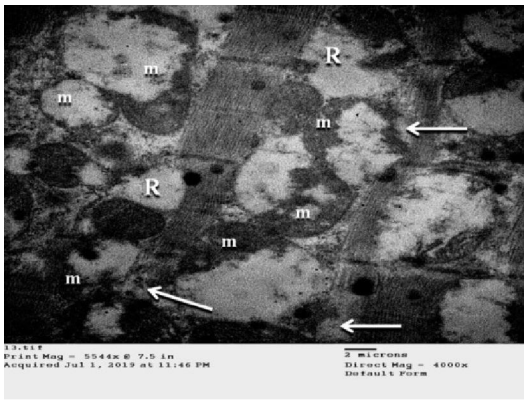

Fig.14: An electron micrograph of a section of a rat myocardium from group II showing markedly disturbed myocardial architecture with disrupted myofibrils (arrow), extensive sarcoplasmic rarefaction (R). All mitochondria appear ballooned with lost cristae (m) **(TEM X4000).**

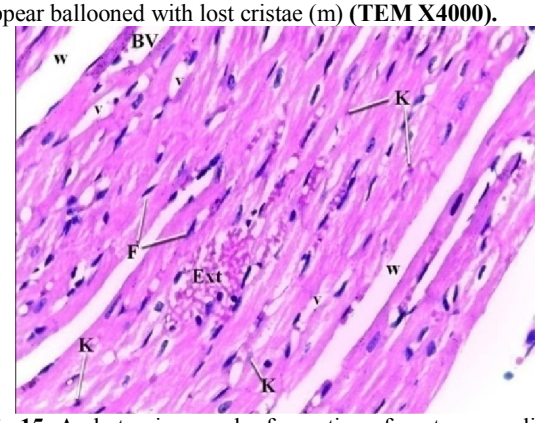

Fig.15: A photomicrograph of a section of a rat myocardium from group **III (Diabetic rats treated with insulin)** showing apparently normal pattern of myocardial fibers, fairly widened interstitial spaces (W), mildly increased fibroblasts (F) and extravasted blood (Ext), Few areas of sarcoplasmic vacuolation (v) and few karyolitic nuclei (K) can be seen **(H & E 400).**

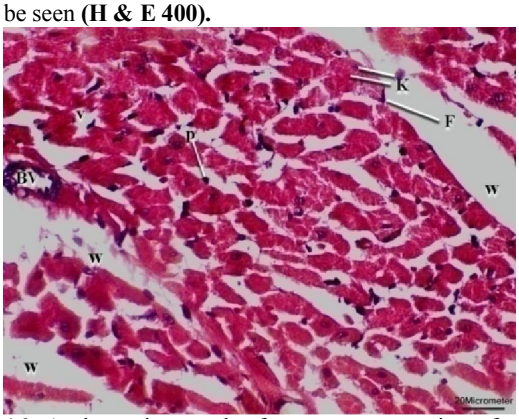

Fig.16: A photomicrograph of a transverse section of a rat myocardium from group **III** showing apparently normal pattern of myocardial fibers, fairly widened interstitial spaces (W), with moderately thickened blood vessel (BV), mildly increased fibroblasts (F). Few areas of sarcoplasmic vacuolation (v), Few karyolitic (K) and Pyknotic (p) nuclei can be seen **(H & E 400).**

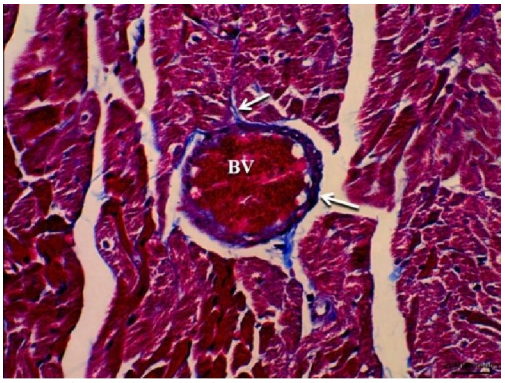

Fig.17: A photomicrograph of a section of a rat myocardium from group III displaying moderate increase in collagen tissue deposition (arrow) between myocardial fibers and around a markedly congested blood vessel **(BV) (Masson's trichrome x 400).**

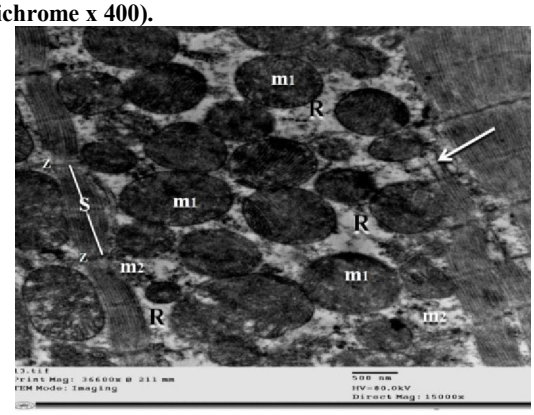

Fig.18: An electron micrograph of a section of a rat myocardium from group III showing some apparently normal myofibrils; a sarcomer (S) between two successive Z lines, disrupted myofibrils (arrow), extensive sarcoplasmic rarefaction (R). Pathological aggregation of mitochondria that are apparently normal with intact cristae (m1) or ballooned with lost cristae (m2) **(TEM X15000).**

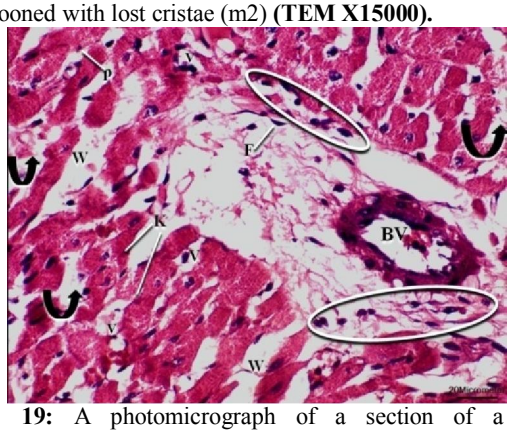

Fig. 19: A photomicrograph of a section of a rat myocardium from group **(Diabetic rats treated with captopril) IV** showing markedly widened interstitial spaces (W) and increased fibroblast (F), disrupted myocardial fibers (curved arrow), mononuclear cell infiltration (Inf) around a thickened blood vessel (BV). Sarcoplasmic vacuolation (v), pyknotic (P) and karyolitic (K) nuclei can be visualized **(H & E X 400).**

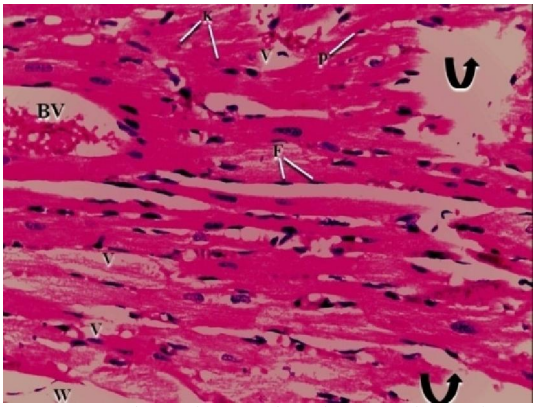

Fig. 20: A photomicrograph of a section of a rat myocardium from group **IV** showing markedly increased fibroblast (F), severely disrupted myocardial fibers (curved arrow), a moderately congested blood vessel (BV). Sarcoplasmic vacuolation (v), pyknotic (P) and karyolitic (K) nuclei can be visualized **(H & E X 400).**

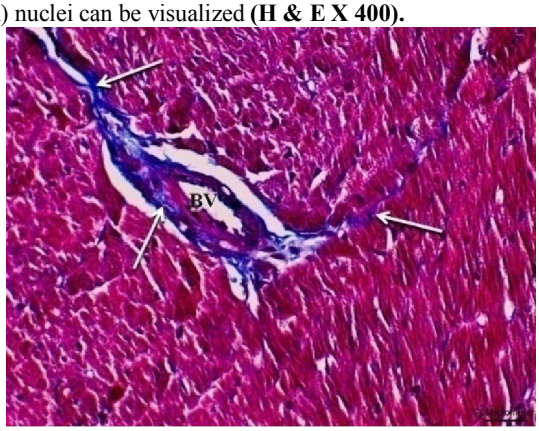

Fig.21: A photomicrograph of a section of a rat myocardium from group **IV** displaying marked increase in collagen tissue deposition (arrow) between myocardial fibers and around blood vessels **(BV) (Masson's trichrome x 400).**

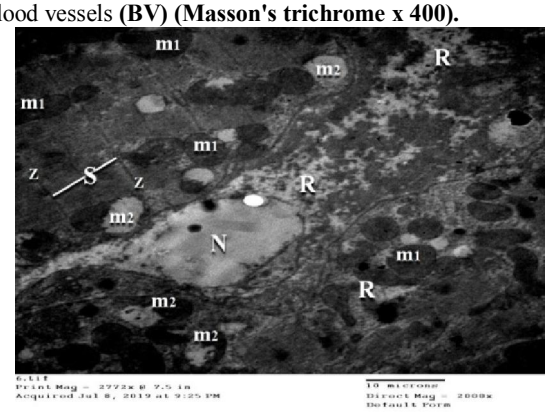

Fig.22: An electron micrograph of a section of a rat myocardium from group IV showing extremely shrunken and karyolitic nucleus (N), marked sarcoplasmic rarefaction (R), some apparently normal myoibrils; a sarcomere (S) between 2 successive Z lines. The mitochondria are either apparently normal with intact cristae (m1) or mostly ballooned with lost cristae **(TEM x2000).**

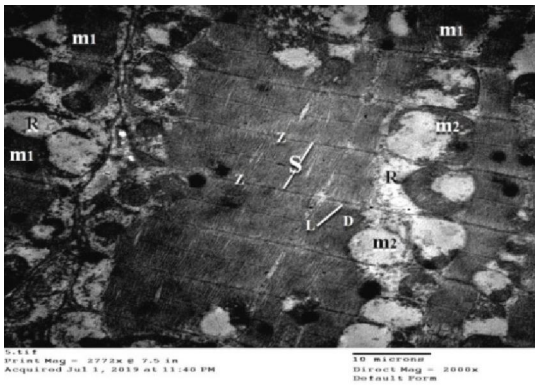

Fig.23: An electron micrograph of a section of a rat myocardium from group IV showing sarcoplasmic rarefaction (R), apparently normal myoibrils; alternating dark bands (D) and light bands (L) with regular Z lines inside and a sarcomere (S) between 2 successive Z lines. The mitochondria are either apparently normal with intact cristae (m1) or mostly ballooned with lost cristae **(TEM x2000).**

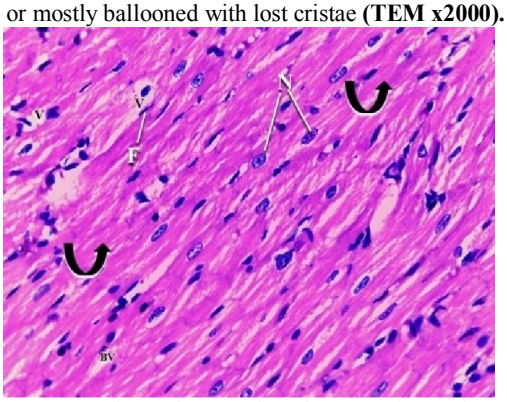

Fig. 24: A photomicrograph of a section of a rat myocardium from group **V (Diabetic rats treated with insulin and captopril)** showing apparently normal pattern of myocardial fibers and their nuclei (N), Few spindle shaped nuclei of fibroblast in the interstitial tissue in-between (F) and small thin walled blood vessels (BV). Few areas of sarcoplasmic vacuolation (v) can be seen **(H & E 400).**

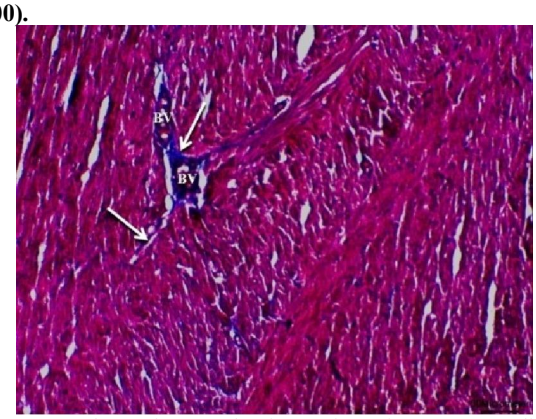

Fig.25: A photomicrograph of a section of a rat myocardium from group V displaying apparently normal distribution of in collagen tissue (arrow) between myocardial fibers and around blood vessels **(BV) (Masson's trichrome x 200).**

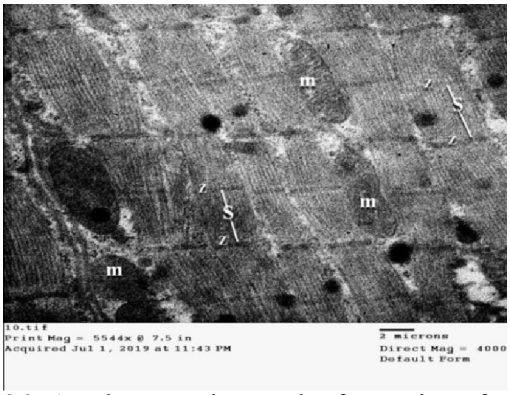

Fig.26: An electron micrograph of a section of a rat myocardium from group V showing apparently normal myocardial architecture; a sarcomere (S) between 2 successive Z lines. The mitochondria are apparently normal with intact cristae (m) **(TEM x4000).**

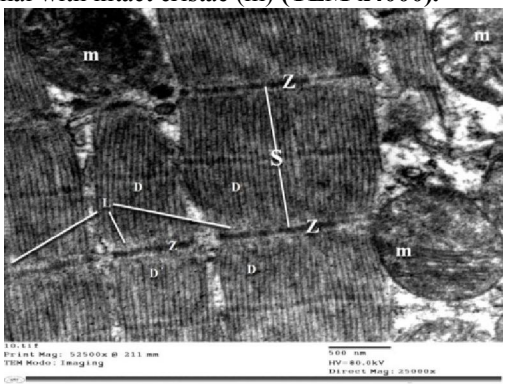

Fig.27: An electron micrograph of a section of a rat myocardium from group V showing apparently normal myocardial architecture; alternating dark bands (D) and light bands (L) with regular Z lines inside and sarcomere (S) between 2 successive Z lines. The mitochondria are apparently normal with intact cristae (m) **(TEM x4000).**

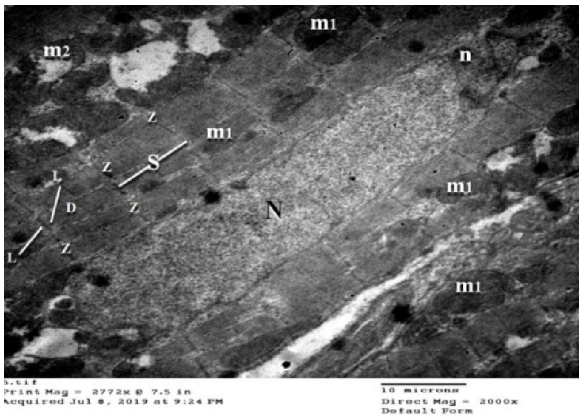

Fig.28: An electron micrograph of a section of a rat myocardium from group V showing euchromatic nucleus (N) with a prominent nucleolus (n), apparently normal myocardial architecture**;** alternating dark bands (D) and light bands (L) with regular Z lines inside and sarcomere (S) between 2 successive Z lines. Most of mitochondria are apparently normal with intact cristae (m1), however few of them are ballooned with lost cristae (m2) **(TEM x4000).**

Fig. 29: A table of area percent of collagen fibers in rat heart obtained from different groups of the examined animals.

	Group I (Control)		**Group II**		**Group III**		**Group IV**		**Group V**	
	Mean	**SD**	**Mean**	**SD**	**Mean**	**SD**	**Mean**	**SD**	**Mean**	**SD**
Collagen area %	2.35	0.49	19.53	5.02	10.12	1.16	13.94	1.6	3.86	1.35
P-values										
G I vs. G II	**<0.0001 (S)**									
G I vs. G III	**0.001 (S)**									
G I vs. G IV	**<0.0001 (S)**									
G I vs. G V	0.870 (NS)									
G II vs. G III			**<0.0001 (S)**							
G II vs. G IV			**0.016 (S)**							
G II vs. G V			**<0.0001 (S)**							
G III vs. G IV					0.150 (NS)					
G III vs. G V					**0.006 (S)**					
G IV vs. G V							**<0.0001 (S)**			

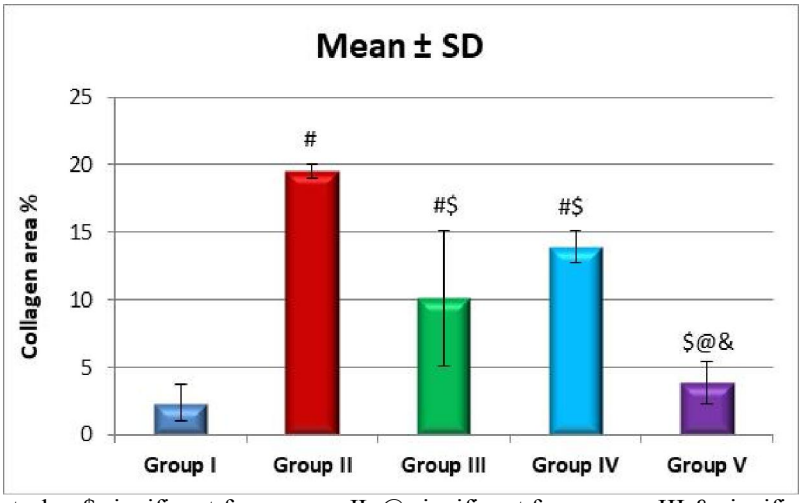

significant from control, m$ significant from group II, @ significant from group III & significant from IV

Fig. 30: Histogram: illustrating mean distribution of the connective tissue **(area percent)** between the myocardial fibers in heart specimens obtained from the different groups of the examined animals.

Fig. 31: A table demonstrating mean values of **glutathione peroxidase** among different study groups.

	Group I (Control)		**Group II**		**Group III**		**Group IV**		**Group V**	
	Mean	**SD**	**Mean**	**SD**	**Mean**	**SD**	**Mean**	**SD**	**Mean**	**SD**
glutathione peroxidase	60.04	5.74	17.78	1.98	42.4	3.86	33.28	4.3	51.81	2.29
P-values										
G I vs. G II	**<0.0001 (S)**									
G I vs. G III	**<0.0001 (S)**									
G I vs. G IV	**<0.0001 (S)**									
G I vs. G V	**0.024 (S)**									
G II vs. G III			**<0.0001 (S)**							
G II vs. G IV			**<0.0001 (S)**							
G II vs. G V			**<0.0001 (S)**							
G III vs. G IV					**0.011 (S)**					
G III vs. G V					**0.008 (S)**					
G IV vs. G V							**<0.0001 (S)**			

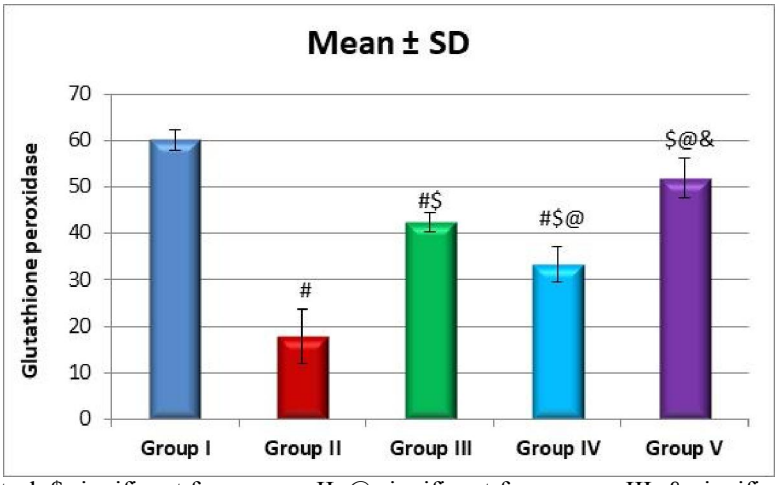

significant from control, $ significant from group II, @ significant from group III, & significant from IV

Fig. 32: Histogram: illustrating mean values of **glutathione peroxidase** obtained from the different groups of the examined animals.

Fig. 33: A table demonstrating mean values of **superoxide dismutase** among different study groups.

	Group I (Control)		Group II		Group III		Group IV		Group V	
	Mean	**SD**	**Mean**	**SD**	**Mean**	**SD**	**Mean**	**SD**	**Mean**	**SD**
Superoxide dismutase (SOD	4.02	0.28	0.96	0.25	2.32	0.38	1.8	0.26	3.19	0.26
P-values										
G I vs. G II	**<0.0001 (S)**									
G I vs. G III	**<0.0001 (S)**									
G I vs. G IV	**<0.0001 (S)**									
G I vs. G V	**0.002 (S)**									
G II vs. G III			**<0.0001 (S)**							
G II vs. G IV			**0.001 (S)**							
G II vs. G V			**<0.0001 (S)**							
G III vs. G IV					0.067 (NS)					
G III vs. G V					**0.001 (S)**					
G IV vs. G V							**<0.0001 (S)**			

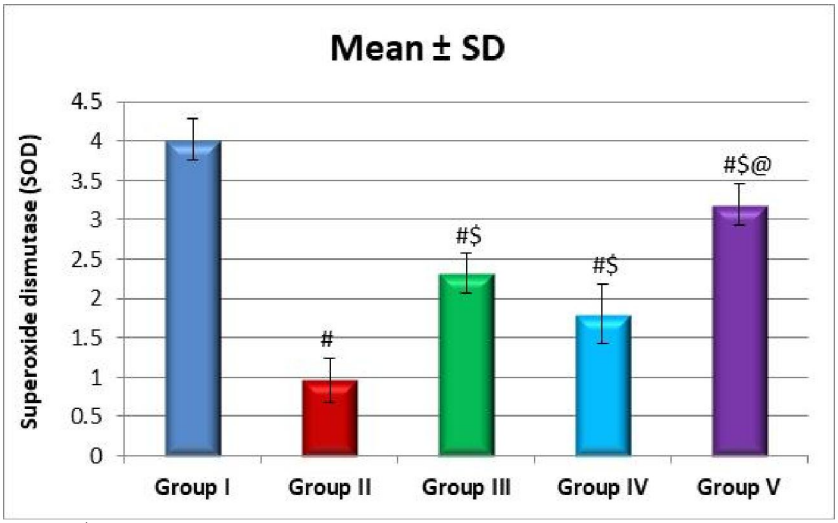

significant from control, $ significant from group II, @ significant from group III & significant from IV

Fig. 34: Histogram: illustrating mean values of **superoxide dismutase** obtained from the different groups of the examined animals.

Fig. 35: A table illustrating mean values of: Vascular endothelial growth factor **VEGF** in rat heart using Polymerase chain reaction technique (PCR) among different study groups

	Group I (Control)		Group II		Group III		Group IV		Group V	
	Mean	**SD**	**Mean**	**SD**	**Mean**	**SD**	**Mean**	**SD**	**Mean**	**SD**
Heart VEGF	1.28	0.35	0.53	0.31	2.44	0.51	1.96	0.55	5.39	0.54
P-values										
G I vs. G II	0.116 (NS)									
G I vs. G III	**0.006(S)**									
G I vs. G IV	0.183 (NS)									
G I vs. G V	**<0.0001 (S)**									
G II vs. G III			**<0.0001 (S)**							
G II vs. G IV			**0.001 (S)**							
G II vs. G V			**<0.0001 (S)**							
G III vs. G IV					0.481 (NS)					
G III vs. G V					**<0.0001 (S)**					
G IV vs. G V							**<0.0001 (S)**			

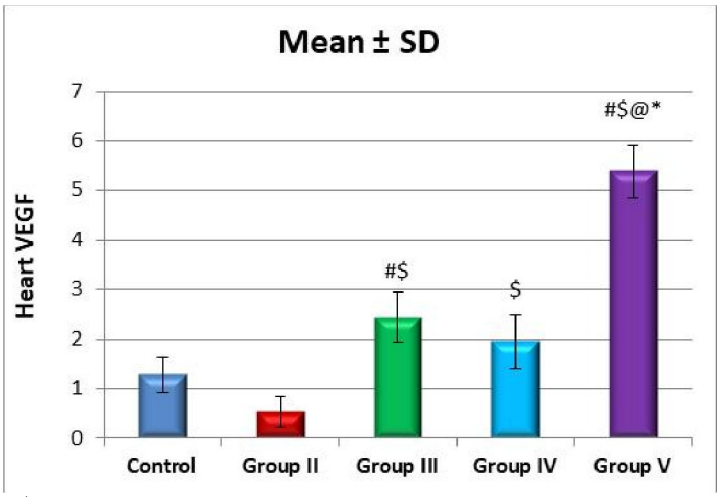

significant from control, $ significant from group II, @ significant from group III,* significant from group IV

Fig. 36: Histogram: illustrating mean values of **VEGF** in rat heart obtained from the different groups of the examined animals.

Fig. 37: A table illustrating mean values of: **VEGF** in rat kidney using PCR among different study groups

	Group I (Control)		**Group II**		**Group III**		**Group IV**		**Group V**	
	Mean	**SD**	**Mean**	**SD**	**Mean**	**SD**	**Mean**	**SD**	**Mean**	**SD**
Kidney VEGF	0.94	0.23	4.01	0.29	2.40	0.38	3.16	0.51	1.87	0.15
P-values										
G I vs. G II	**<0.0001 (S)**									
G I vs. G III	**<0.0001 (S)**									
G I vs. G IV	**<0.0001 (S)**									
G I vs. G V	**0.003 (S)**									
G II vs. G III			**<0.0001 (S)**							
G II vs. G IV			**0.005 (S)**							
G II vs. G V			**<0.0001 (S)**							
G III vs. G IV					**0.014 (S)**					
G III vs. G V					0.134 (NS)					
G IV vs. G V							**<0.0001 (S)**			

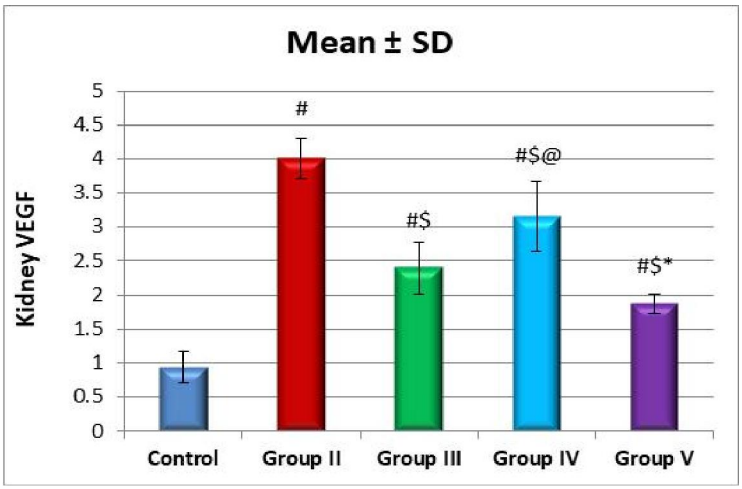

significant from control, $ significant from group II,@ significant from group III* significant from group IV

Fig. 38: Histogram: illustrating mean values of **VEGF** in rat kidney obtained from the different groups of the examined animals.

Fig. 39: A table illustrating mean values of: **VEGF** in rat retina using PCR among different study groups

	Group I (Control)		**Group II**		**Group III**		**Group IV**		**Group V**	
	Mean	**SD**	**Mean**	**SD**	**Mean**	**SD**	**Mean**	**SD**	**Mean**	**SD**
Retina VEGF	0.96	0.21	3.94	0.13	2.66	0.43	3.02	0.6	1.62	0.38
P-values										
G I vs. G II	**<0.0001 (S)**									
G I vs. G III	**<0.0001 (S)**									
G I vs. G IV	**<0.0001 (S)**									
G I vs. G V	0.098 (NS)									
G II vs. G III			**<0.0001 (S)**							
G II vs. G IV			**0.013 (S)**							
G II vs. G V			**<0.0001 (S)**							
G III vs. G IV					0.603 (NS)					
G III vs. G V					**0.004 (S)**					
G IV vs. G V							**<0.0001 (S)**			

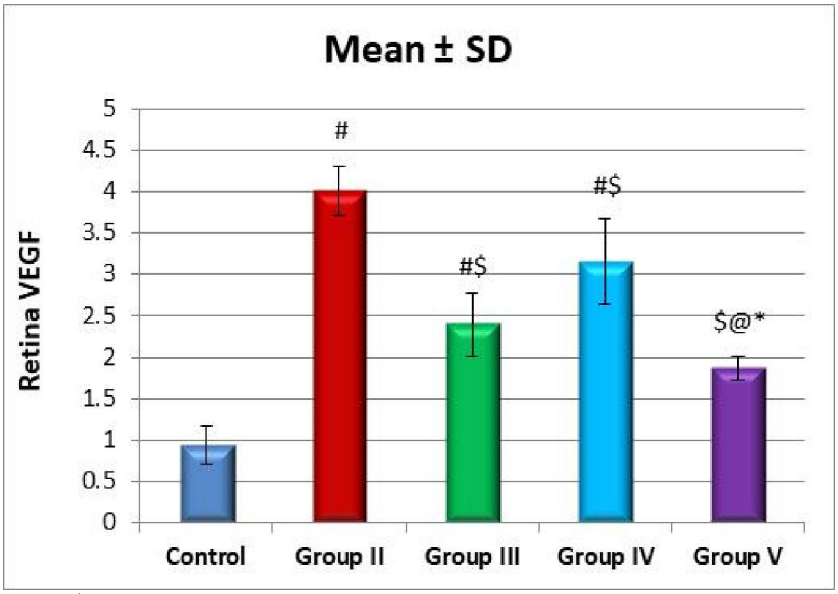

significant from control,$ significant from group II, @ significant from group III * significant from group IV

Fig. 40: Histogram: illustrating mean values of **VEGF** in rat retina obtained from the different groups of the examined animals.

4. Discussion:

In the current study, streptozitocin administration has been used for induction of diabetes mellitus and consequently diabetic cardiomyopathy. Histological examination of myocardial specimens of diabetic rats featured nuclear degeneration in the form of shrinkage, pyknosis and karyolysis, sarcoplasmic vacuolation and rarefaction, mononuclear cell infiltration, congested blood vessels, widening of interstitial spaces, myocardial fibrosis and degenerated mitochondria. This was in agreement with **Fiordaliso et al, 2001 and Al-Jarraha. 2012** who attributed these changes to Angiotensin II synthesis, and ROS overproduction and glycosylation of protein kinase 53 that has a major role in initiating apoptosis in hyperglycemic rats. They added that ROS are responsible for peroxidation of the myocardial cell membrane phospholipids.

In the current study, the myocardial tissue levels of antioxidant enzymes; GPD and SOD were significantly low in diabetic groups in comparison to the normal control group. However, insulin and captopril administration markedly elevated tissue levels of those enzymes again particularly when co-administrated to diabetic rats. The decreased tissue levels of GPD and SOD in diabetic rats was explained by **Solaini and Harris, 2005; Yin et al, 2011 who stated that** decreased GPD activity is a result of overproduction of ROS in rat myocardium and exhaustion of glutathione stores in myocardial fibers resulting in impairment of antioxidant defences**.**

In the current study, disrupted myocardial fibers and nuclear pyknosis in diabetic rats have been observed. Similar findings were detected by **Abdel Hamid et al, 2017 who** attributed them to decreased cell metabolism and beginning of an apoptotic pathway.

In the current work, widened spaces between cardiac muscle fibers was detected in diabetic rats. A similar result was found by **Dyntar et al, 2006** who attributed this to the lack of cellular cohesion leading to heart dysfunction. Myocardial fibrosis was evident in diabetic rats in the present work. This was in agreement with **Fedak et al, 2003** who referred this fibrosis to interstitial collagen to replace degenerated cardiomyocytes as a compensatory mechanism of cell regeneration and process of tissue healing following cell damage.

In the present work, examination of specimens of diabetic rats treated with captopril revealed mild improvement of histological alterations and tissue levels of GPD and SOD. This was in agreement with **Rostagno et al, 2008 who stated that** captopril has a cardioprotective effect in autoimmune myocarditis. infection-induced cardiomyopathy and drug-induced cardiomyopathy. **Opie and Sack, 2001; Godsel et al, 2003; Leon et al, 2003 and Scribner et al, 2003; Sacco et al, 2009** reported that captopril has antioxidant properties due to presence of its sulfhydryl group that is able to neutralize ROS either by a donation of hydrogen or by an electron-transfer mechanism. Also, it attenuates the effect of Angiotensin II involved in inflammation, myocarditis, endothelial dysfunction, and heart failure. They added that captopril has immunomodulatory functions because it regulates chemotaxis, differentiation, activation, adhesion and the production of cytokine immune cells.

In the present work, examination of heart specimens of diabetic rats treated with insulin revealed that the myocardial damage was obviously improved compared with the diabetic group. The combination of both insulin and captopril showed an obvious improvement of myocardial injury compared with the diabetic rats. This was in agreement with **Singh et al, 2008** who recorded that combination of insulin therapy with angiotensin converting enzyme inhibitors resulted in markedly elevated tissue levels of antioxidant enzymes, decreased tissue fibrosis and myocardial injury.

In the current work, administration of insulin to diabetic rats markedly improved cardiomyocyte degeneration and tissue levels of GPD and SOD more than captopril when used alone. This was in agreement with **Frustaci et al, 2000**, who stated that cardiomyocyte apoptosis is controlled with blood glucose level.

In the current study, diabetic rats exhibited downregulation of cardiac VEGF. However, diabetic rats treated with insulin and captopril presented upregulation of VEGF especially in rats treated with both insulin together with captopril more than rats treated with insulin or captopril alone. This was in line with **Chou et al, 2002** and **Dubó et al, 2016** who stated that formation of hypoxia-induced collateral vessels is decreased in myocardium of diabetic rats and consequently decreased expression of VEGF. The paradoxical changes in VEGF expression and its receptors indicate that local regulatory factors are present in myocardium. They added that there was a decrease in VEGF and its receptors, suggesting causes other than hypoxia. Moreover, insulin-resistant and glucose intolerance may reduce the expression of VEGF in myocardium. This might explain the clinical findings that early cardiomyopathy occurs in patients with insulin resistance and diabetics, While retinal and glomerular lesions are usually lower for several years until the establishment of frank hyperglycemia. In addition, Loss of insulin-induced VEGF expression is a possible cause for decreased VEGF expression in myocardium in diabetic states.

Escudero et al, 2017 reported that insulin causes vasorelaxation, improves amino acid endothelial absorption e.g. L-arginine, which enhances endothelial cell viability and migration. As a result, insulin can enhance expression of proangiogenic factors such as VEGF, as well as increasing the survival of pericytes and reducing the expression of anti-angiogenic proteins. They added that diabetes mellitus exerts differential expression of VEGF and its receptors depending on the cell type and duration of diabetes mellitus and insulin can norrnalize VEGF expression in different tissues.

On the other hand, in the current study, diabetic rats exhibited upregulation of renal and retinal VEGF. However, diabetic rats treated with insulin and captopril presented downegulation of VEGF especially in rats treated with both insulin together with captopril more than rats treated with insulin or captopril alone. This was in accordance with **Chou et al, 2002** who found the same results in their study on both kidney and retina. It has been documented that hyperglycemia induces VEGF expression through increased oxidants and glycation products. With the initiation of acute hyperglycemia, VEGF rises and their receptors have become more noticeable, consistent with clinical findings that the main risk factor for diabetic retinopathy and nephropathy is glycemic control.

References:

1. Abdel Hamid, O.I.; Ahmed, M.G.; Hassaneine, H.M.A. and Hayam E Rashed, H.E. (2017): Evaluation of the role of captopril on clozapine-

induced cardiotoxicity and hematotoxicity in adult male albino rats. Toxicology Research and Application, 1: 1–11.
2. Abuissa, H.; Jones, P.G.; Marso, S.P. and O'Keefe, J.J.H. (2005): Angiotensinconverting enzyme inhibitors or angiotensin receptor blockers for prevention of type 2 diabetes: a meta-analysis of randomized clinical trials. J. Am. Coll. Cardiol., 46:821-6.
3. Al-Jarraha, M. Effect (2012): of exercise training on the expression of p53 and iNOS in the cardiac muscle of type I diabetic rats. J. Endocrinol. Metab, 2:176–180.
4. Andraws, R. and Brown, D.L. (2007): Effect of inhibition of the renin-angiotensin system on development of type 2 diabetes mellitus (metaanalysis of randomized trials). Am. J. Cardiol., 99:1006-12.
5. Balkis, B. S.; Othman, F.; Louis, S.R.; Abu Bakar, M.; Radzi, M. and Osman, K. (2009): Effect of alpha lipoic acid on oxidative stress and vascular wall of diabetic rats. Rom J. Morphol. Embryol., 50:23–30.
6. Benter, I.F.; Yousif, M.H.M.; Al-Saleh, F.M.; Raghupathy, R.; Chappell, M.C. and Diz, D.I. (2011): angiotensin-(1-7) blockade attenuates Captopril- or Hydralazine induced cardiovascular protection in spontaneously hypertensive ratstreated with L-NAME. J. Cardiovasc. Pharmacol., 57:559–567.
7. Calvi, E.N.V.; Nahas, F.X.; Barbosa, M.V.; Calil, J.A.; Ihara, S.S.M.; Silva, M.S.; De Franco, M.F. and Ferreira, L.M. (2012): An experimental model for the study of collagen fibers in skeletal muscle. Acta Cirúrgica Brasileira, 27 (10): 681-686.
8. Chou, E; Suzuma,I.; Way, K. J.; Opland, D.; Clermont, A.C.; Naruse, K.; Suzuma, K.; Bowling, N.L.; Vlahos, C.J.; Aiello, L.P.; King, G.L. (2002): Decreased Cardiac Expression of Vascular Endothelial Growth Factor and Its Receptors in Insulin-Resistant and Diabetic States: A Possible Explanation for Impaired Collateral Formation in Cardiac Tissue. Circulation, 105:373-379.
9. Dubó, S.; Gallegos, D.; Cabrera, L.; Sobrevia, L.; Zúñiga, L., and González, M. (2016). Cardiovascular action of insulin in health and disease: endothelial larginine transport and cardiac voltage-dependent potassium channels. Front. Physiol., 7:74.
10. Dyntar, D.; Sergeev, P. and Klisic, J. (2006): High glucose alters cardiomyocyte contacts and inhibits myofibrillar formation. J. Clin. Endocrinol. Metab., 98(13): 1329–1334.
11. Escudero, C.A,; Herlitz, K.; Troncoso, F.; Guevara, K.; Acurio, J.; Aguayo, C.; Godoy, A.S. and González, M. (2017): Pro-angiogenic Role of Insulin: From Physiology to Pathology. Front. Physiol., 8: 204.
12. Esteva, S.; Panisello, P.; Casas, M.; Torrella, J.R.; Pagés, T. and Viscor, G. (2008): Morphofunctional responses to anaemia in rat skeletal muscle. Journal of Anatomy, 212: 836-844.
13. Falcão-Pires, I and Leite-Moreira, A.F. (2012): Diabetic cardiomyopathy: Understanding the molecular and cellular basis to progress in diagnosis and treatment. Heart Fail. Rev., 17: 325-344.
14. Fedak, P.W.M.; Altamentova, S.M. and Weisel, R.D. (2003): Matrix remodeling in experimental and human heart failure: a possible regulatory role for TIMP-3. Am. J. Physiol. Heart Circ. Physiol., 248(2): 626–634.
15. Fiordaliso, F.; Leri, A.; Cesselli, D.; Limana, F.; Safai, B. and Nadal-Ginard. B. (2001): Hyperglycemia activates p53 and p53-regulated genes leading to myocyte cell death. Diabetes, 50:2363–2375.
16. Frustaci, A.; Kajstura, J.; Chimenti, C.; Jakoniuk, I.; Leri, A. and Maseri, A. (2000): Myocardial cell death in human diabetes. Circ. Res., 87:1123–1132.
17. Godsel, L.M.; Leon, J.S. and Wang, K. (2003): Captopril prevents experimental autoimmune myocarditis. J. Immunol., 171: 346–352.
18. Leon, J.S.; Wang, K. and Engman, D.M. (2003): Captopril ameliorates myocarditis in acute experimental Chagas disease. Circulation, 107(17): 2264–2269.
19. Liu, J.; Jha, P.; Lyzogubov, V.V.; Tytarenko, R.G.; Bora, N.S. and Bora, P.S. (2011): Relationship between Complement Membrane Attack Complex, Chemokine (C-C Motif) Ligand 2 (CCL2) and Vascular Endothelial Growth Factor in Mouse Model of Laser-induced Choroidal Neovascularization. The Journal of Biological Chemistry, 286(23): 20991–21001.
20. McGuire, D.K.; Winterfield, J.R.; Rytlewski, J.A. and Ferrannini, E. (2008): Blocking the renin-angiotensin-aldosterone system to prevent diabetes mellitus. Diab. Vasc. Dis. Res., 5:59-66.
21. Michael, T.; Ganesh, N. and Viswanathan, P. (2012): Effect of long acting insulin supplementation on diabetic nephropathy in Wistar rats. Indian J. Experim. Biol., 50:867–874.
22. Mikrut, K.; Kupsz, J.; Koźlik, J.; Krauss, H.; Pruszyńska-Oszmałek, E. And Dorna, M.G. (2016): Angiotensin-converting enzyme

inhibitors reduce oxidative stress intensity in hyperglicemic conditions in rats independently from bradykinin receptor inhibitors. Croat Med. J., 57:371-380.
23. Munzel, T. and Keaney, J.F. J. (2001): Are ACE inhibitors a "magic bullet" against oxidative stress? Circulation, 104:1571-1574.
24. Neamati, S.; Alirezaei, M.; Kheradmand, A.; Rashidipour, M. and Saki, M.R. (2013): Antioxidant enzyme activities assay and thiobarbituric acid reactive substances concentration following administration of ghrelin in the rat kidney. International Journal of Pharmacy Teaching & Practices,4 (1): 451-457.
25. Opie, L.H. and Sack, M.N. (2001): Enhanced angiotensin II activity in heart failure – reevaluation of the counter regulatory hypothesis of receptor subtypes. Circ. Res., 88(7): 654–658.
26. Patel, L. and Thaker, A. (2015): The effects of A2B receptor modulators on vascular endothelial growth factor and nitric oxide axis in chronic cyclosporine nephropathy. Journal of Pharmacology and Pharmacotherapeutics, 6 (3): 147- 153.
27. Rostagno, C.; Di Norscia, G. and Placidi, G.F. (2008): Beta-blocker and angiotensin-converting enzyme inhibitor may limit certain cardiac adverse effects of clozapine. Gen. Hosp. Psychiat., 30(3): 280–283.
28. Sacco, G.; Bigioni, M. and Lopez, G. (2009): ACE inhibition and protection from doxorubicin-induced cardiotoxicity in the rat. Vasc. Pharmacol., 50(5–6): 166–170.
29. Scribner, A.W.; Loscalzo, J. and Napoli, C. (2003): The effect of angiotensin-converting enzyme inhibition on endothelial function and oxidant stress. Eur. J. Pharmacol., 482(1–3): 95–99.
30. Singh, V.; Le, B.; Khode, R.; Baker, K.M. and Kumar, R. (2008): Intracellular angiotensin ii production in diabetic rats is correlated with cardiomyocyte apoptosis, oxidative stress, and cardiac fibrosis. Diabetes, 57:3297–3306.
31. Shiju, T.M.; Rajesh, N.G. and Pragasam, V. (2012): Effect of long acting insulin supplementation on diabetic nephropathy in Wistar rats. Ind. J. Exp. Histol., 50:867–874.
32. Solaini, G. and Harris, D.A. (2005): Biochemical dysfunction in heart mitochondria exposed to ischaemia and reperfusion. Biochem. J., 390: 377–394.
33. Wen, Y.; Ouyang, J.; Yang, R.; Chen, J.; Liu, Y. and Zhou, X. (2008): Reversal of new onset type 1 diabetes in mice by synergic bone marrow transplantation. Bioch. Biophy. Res. Commu., 374:282–287.
34. Westermann, D.; Walther, T.; Savvatis, K.; Escher, F.; Sobirey, M.; Riad, A.; Bader, M.; Schultheiss, H.P. and Tschöpe, C. (2009): Gene deletion of the kinin receptor B1 attenuates cardiac inflammation and fibrosis during the development of experimental diabetic cardio-myopathy. Diabetes, 58: 1373-1381.
35. Yin, H.; Xu, L. and Porter, N.A. (2011): Free radical lipid peroxidation: mechanisms and analysis. Chem. Rev., 11(10): 5944–5972.
36. Zheng, W.; Li, D.; Gao, X.; Zhang, W. and Robinson, B.O. (2019): Carvedilol alleviates diabetic cardiomyopathy in diabetic rats. Experimental and therapeutic medicine, 17: 479-487.

8/25/2020